Prediction of mechanical properties of Electron Beam Melted Ti6Al4V parts using dislocation density based crystal plasticity framework

Deepankar Pal, Nachiket Patil and Brent E. Stucker
Department of Industrial Engineering, University of Louisville, KY 40292

Abstract

Parts produced using Electron Beam Melting (EBM) with Ti6Al4V powders are generally tested for two important mechanical properties, namely tensile strength and fatigue life. The optimization of the process input parameters, such as part orientation, initial powder size and hatch pattern, for the abovementioned mechanical properties has been attempted using two numerical finite element methods. First, the dislocation density based crystal plasticity framework (DDCP-FEM) has been used to evaluate the localized stress-strain evolution, dislocation density evolutions and non-local deformations as a function of loading, sample geometry, microstructural phase, grain size and shape. This analysis has been compared against simulations based on continuum plasticity based finite element techniques. Though the localized evolutions as a function of microstructural attributes are missing in the continuum analysis, the low computational costs involved makes this technique an ideal candidate for spatial homogenization of the DDCP-FEM framework. The simulations conducted in the current work only validate the mechanical properties for tensile and fatigue specimens fabricated with known process parameters. These simulations will form the basis for future modeling efforts to optimize these parameters for required mechanical properties in service.

Introduction

Electron Beam Melting (EBM) is a metal powder bed fusion additive manufacturing technology capable of fabricating complex parts required in a number of industrial sectors including aerospace, defense and medical implant industries. For fabrication using the EBM process, first a 3-dimensional solid model of the part is drafted. The abovementioned 3-dimensional geometry is subsequently sliced into 2–dimensional layers which can accommodate internal geometries such as internal cooling channels during fabrication. The parts are built up layer-by-layer using an electron beam on a powder bed. Each layer is melted to the geometry defined by the solid model. The entire process takes place in vacuum for low electron scattering and at a high temperature for low temporal thermal gradient between the localized melt pool and surrounding powder; for low residual stresses in the final part along-with coherent microstructural phases such as hexagonally close packed (HCP) α and body centered cubic (BCC) β phases.

It has been observed in the recent past that Titanium alloys processed using EBM, found acceptance primarily in the medical implant industry for manufacturing acetabular cups. Similarly, turbine blades for aero engines using γ-TiAl (Titanium Aluminides) fabricated by EBM have already entered the production stage [1]. With the advent of these applications and growing number of materials getting processed using EBM for manufacturing commercially usable parts, it is necessary that a numerical simulation tool should be formulated that can correlate the build parameters, orientation and resulting microstructures with the mechanical

properties of the parts produced. Henceforth, this numerical tool could be used for tweaking the build parameters and orientation according to the design requirements (strength and geometry) and service life (high cycle fatigue).

Keeping the above-mentioned objectives in mind, an attempt has been made in this paper to model the microscopic deformation response of EBM produced Ti6Al4V parts. Though the final EBM microstructure of Ti6Al4V is comprised of HCP α and BCC β phases, the β phase is very finely dispersed with significantly less volume fraction [2] and hence this initial modeling infrastructure has been developed with HCP α only. The constitutive equation at this scale has been formulated based on an extension of a dislocation density based constitutive equation for face centered cubic crystals (FCC) [3-8]. The formulation in this context is different from the former since HCP crystals do not have a combination of well-defined densely packed planes and directions in which linear defects such as dislocations can easily glide through known slip systems. These further increase the lattice friction in HCP compared to FCC since they are well-defined dense slip systems. Moreover, the HCP slip systems are not as symmetric as FCC resulting in restricted amount of macroscopic plastic flow.

Experimental Procedure

Figure 1 illustrates the typical Arcam EBM system. The system builds the part layer-by-layer, with each layer comprised of approximately 50-70 μm thick atomized Grade 5 Ti–6Al–4V powder. The EBM system in Figure1 builds parts from the bottom up by scanning the focused electron beam ((2) and (3) numbered circles) at nominally 10^3 mm/s to selectively melt specific areas of the powder bed based upon the 3D-CAD model. Powder is added for each layer from the powder cassettes (4) to the top of the part being built (6) in a vacuum chamber. The powder rake shown at (5) moves laterally between the two cassettes (4) to evenly distribute the powder layers over the surface after each build layer is complete. Beam current, beam intensity, scan rate and scan strategy are set based upon user-selected build profiles that Arcam provides or based upon user experience. Microstructure-property variations can be induced by changing the part-build orientation in which the part can be built. For the current study, both vertical and horizontal ASTM E8M tensile and ASTM E466 fatigue samples with their longitudinal axis parallel and perpendicular to thenormal direction with respect to the build table have been built to verify the simulation results. The microstructures of the horizontally and vertically built samples have been shown in figures 2 and 3 respectively along the cross-sections (XY) perpendicular to the build direction (Z). The prior β grains have a near hexagonal morphology with their characteristic side-lengths equal to 78μm for the horizontal and 65μm for the vertical samples respectively. It has been also observed in the literature that these grains tend to be around 3 layers in height in the build direction [9]. The ASTM E8M samples fabricated during the EBM processing were further machined and subjected to uniaxial tensile testing with an applied strain rate of $2x10^{-3}$/s. The ASTM E466 samples were further machined and subjected to a series of loads ranging from 100 MPa to 500 MPa with an R (minimum/maximum stress) ratio of 0.1. The simulations have been carried out at 340 MPa (experimentally obtained vertical sample fatigue limit) with an R ratio of 0.1.
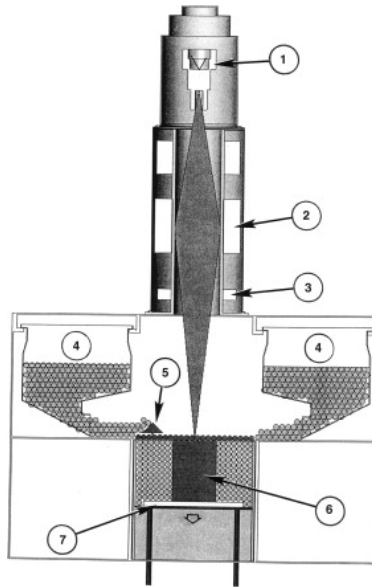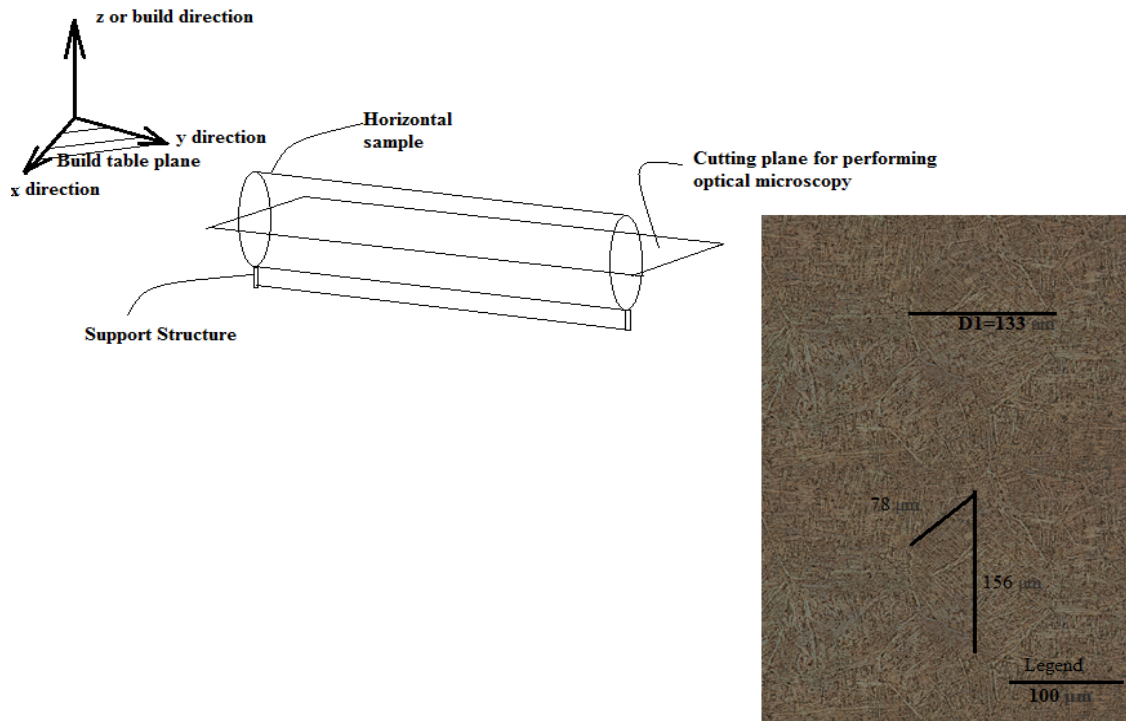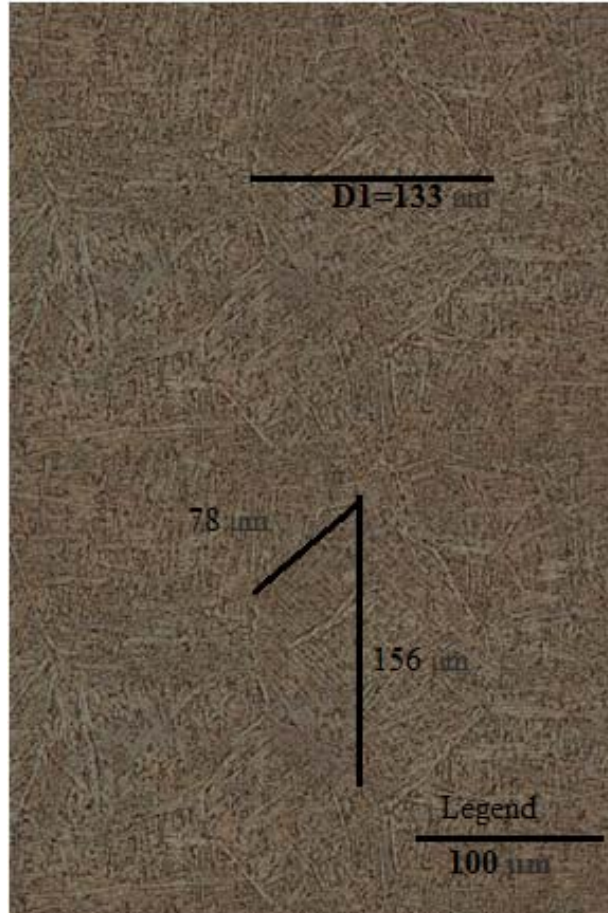
Figure1: EBM system schematic showing key components. The following numbers correspond to those circled in the figure: (1) Electron gun assembly; (2) EB focusing lens; (3) EB deflection coils (x-y); (4) Powder cassettes; (5) Powder layer rake; (6) cylindrical build test specimen; (7) Build table [2]
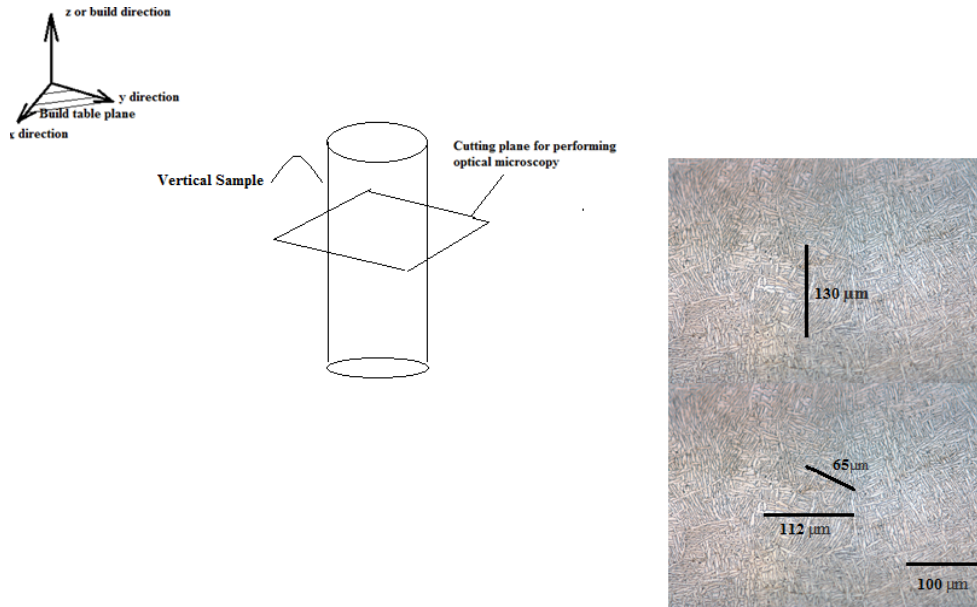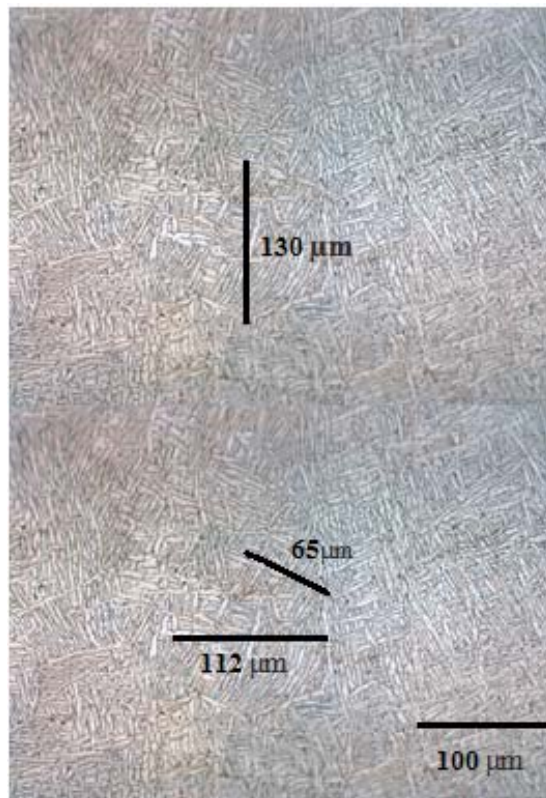

(a)

(b)

Figure2: Optical micrograph of the horizontal sample in the cutting plane perpendicular to the build direction (xy plane perpendicular to z plane according to ASTM F 2921 standard). The tensile and fatigue loading on these samples will be in the direction perpendicular to the build direction. Clearly, a near hexagonal morphology can be seen for these samples with characteristic side-length of the hexagon ~78μm. Optical micrograph taken at 50x.

(a)

(b)

Figure3: Optical micrograph of the vertical sample in the cutting plane perpendicular to the build direction. The tensile and fatigue loading on these samples will be in the direction parallel to the build direction (xy plane perpendicular to z plane according to ASTM F 2921 standard). Clearly,

a near hexagonal morphology can be seen for these samples with characteristic side-length of the hexagon ~65μm. Optical micrograph taken at 50x.

Problem Formulation

1. Dislocation density based flow stress formulation

The problem formulation for flow in a given slip system has been extended from prior work [3-8]. The first difference in the current formulation from the previous formulation is in terms of implementing the slip system geometries of unsymmetrical slip systems in HCP listed in Figure 4 [10]. Miller indices of the slip systems in HCP lattices are described using 4 indices, out of which 3 basal indices are non-orthogonal. Hence, the 4 indices were resolved in terms of 3 orthogonal indices by using projections as shown in figure 5 [10]. The updated miller indices of the families of slip systems in the HCP crystals are listed in Table 1.

Basal-$< a >$
$(0001) < 11\bar{2}0 >, 3$

Prismatic-$< a >$
$\{10\bar{1}0\} < 11\bar{2}0 >, 3$

Pyramidal-$< a >$
$\{10\bar{1}1\} < 11\bar{2}0 >, 6$

1st order Pyramidal-$< c + a >$
$\{10\bar{1}1\} < 11\bar{2}3 >, 12$

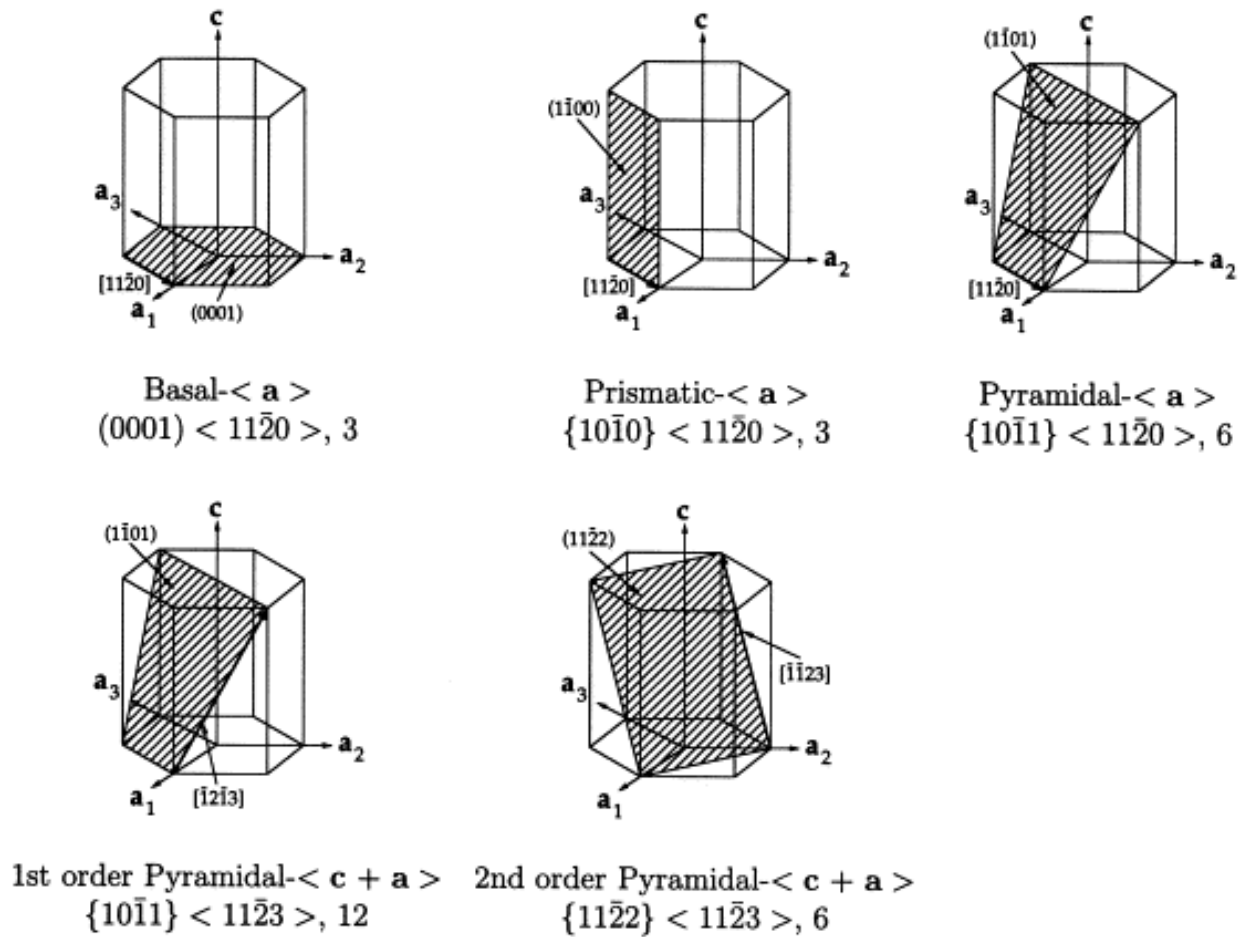2nd order Pyramidal-$< c + a >$
$\{11\bar{2}2\} < 11\bar{2}3 >, 6$

Figure4: Families of slip systems in HCP crystalline lattice [10]
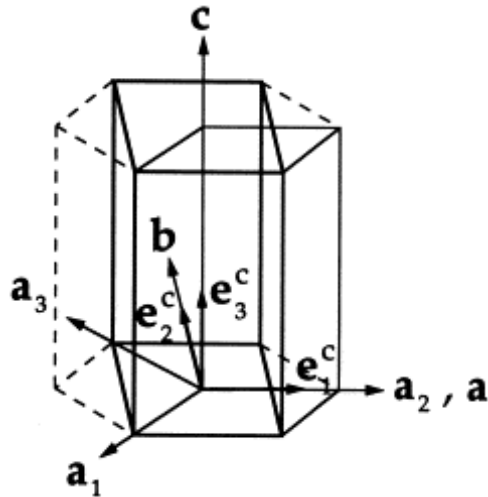
Figure5: Conversion of non-orthogonal slip system basis in HCP crystals using the theory of orthogonal projections [10].

2. Coarse-time scale constitutive modeling of dislocation density based crystal plasticity

The constitutive modeling for coarse time scale evolution of microscopic variables such as dislocation densities, plastic deformation gradient and shear strain rate on a slip system has been extended from 12 symmetric slip systems in FCC described in [11] to 30 for HCP α.

3. Continuum flow formulation

The anisotropic continuum plasticity flow has been captured using the standard anisotropic multilinear model in ANSYS [12].

Results and Discussion

1. Comparison of DDCP-FEM with ANSYS based anisotropic continuum plasticity uniaxial tensile simulations

A representative volume element (RVE) aggregate of 4(x-dir.)×4(y-dir.)×3(z-dir.) grains have been modeled for the vertical sample with its longitudinal axis perpendicular to the build plane using both the DDCP-FEM and ANSYS based anisotropic multilinear plasticity models. The RVE aggregate and the boundary conditions for the simulations are shown in figure 6. The bottom of the geometry has been constrained in all three directions whereas the top surface has been pulled at a constant strain rate of 2×10^{-3}/s. The mesh has been discretized in a hexagonal manner in the cross section perpendicular to the loading direction in order to capture the microstructure. The characteristic side-length of the hexagons has been inserted from the data obtained from figure 2. All the hexagons have been given arbitrary 3-dimensional Bunge-Euler orientations in which the interior HCP α is rotated. The initial dislocation density on all the 30 slip systems of the HCP α has been assumed to be uniformly distributed at $\sim 3.65 \times 10^{12}$. This value is $\sim (1/30)^{th}$ of the aggregate dislocation density measured for these microstructures as shown in figure 7[2].
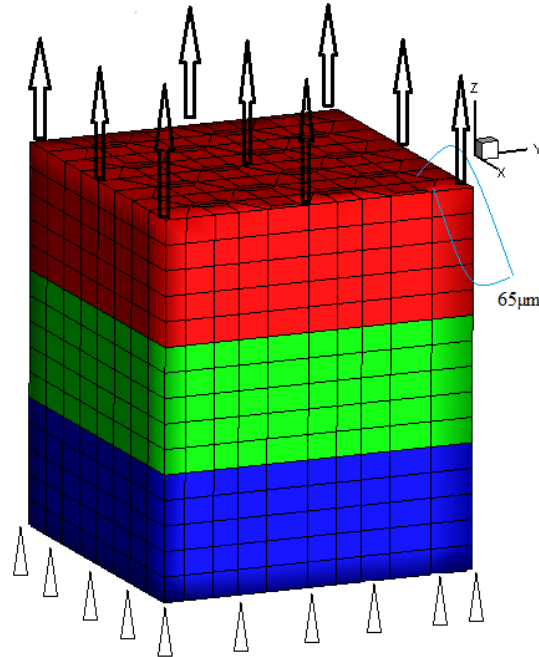
Figure6: Uniaxial tensile boundary conditions and included microstructural morphology for vertical samples. Different colors show grain lengths in the build direction~200μm [9]
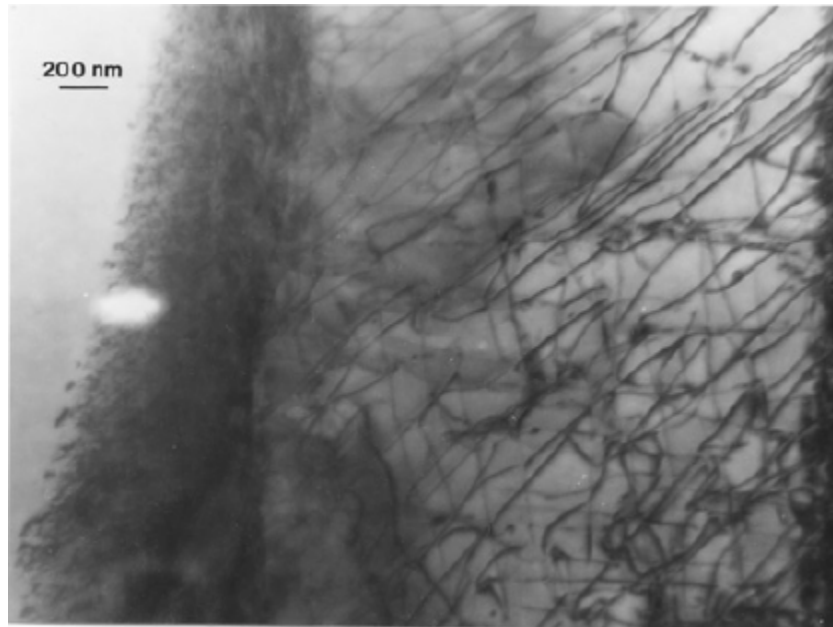

Figure7: Transmission Electron Microscopy (TEM) bright field imaging mode showing the dislocation substructure in HCP α. The total computed dislocation density ~1×10^{14}m/m^3 [2].

The CPU time advantage of ANSYS simulations over DDCP-FEM is around 30 times. This number matches with the number of slip systems to be modeled during the DDCP-FEM simulations for an integration point. The average stress-strain behavior in the loading direction for both the DDCP-FEM and ANSYS simulations also match well with the experiments and have been shown in figure 8. The maximum equivalent plastic strain in the microstructure is also

the same in both the DDCP-FEM and ANSYS simulations and observed to be ~17.88% for an average strain of 10%. However, during the course of simulations DDCP-FEM is more advantageous in assessing the local variation in plastic strain as shown in figure 9. It could be clearly observed that the plastic strain variations are symmetrical and localized about the top center in the ANSYS simulations whereas these variations seem to be a function of grain orientation and slip system phenomenon in DDCP-FEM simulations. Henceforth, the inability of the ANSYS anisotropic continuum plasticity simulations to predict the evolution of plastic strain as a function of Bunge-Euler angle orientations and slip system phenomenon makes it worthless for assessing the mechanical properties of parts produced using EBM in particular and Additive Manufacturing (AM) in general since the involved build phenomenon is highly non-equilibrium in nature leading to complex microstructures governing local and global mechanical properties. The significant time advantage in ANSYS simulations, however, provides impetus for further spatial homogenization of crystal plasticity DDCP-FEM to generate microstructurally informed anisotropic continuum plasticity flow rules.
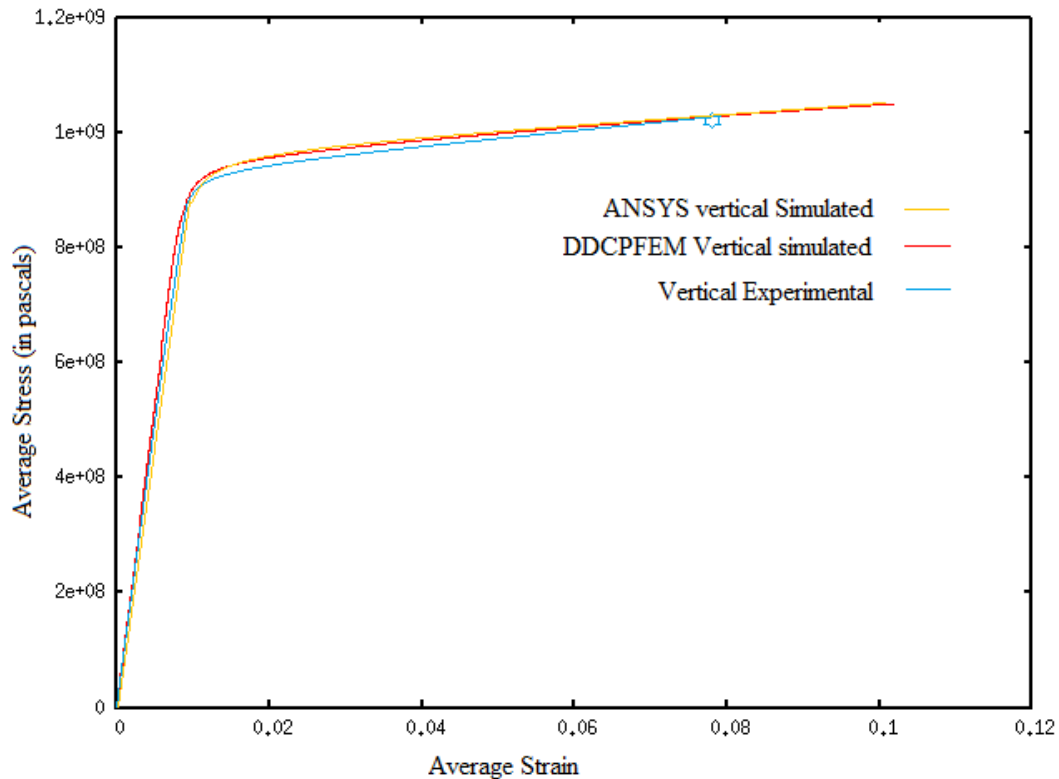

Figure8: Volume averaged true stress-strain plot for vertical sample computed by ANSYS (orange), DDCPFEM (red) and experimental (blue)
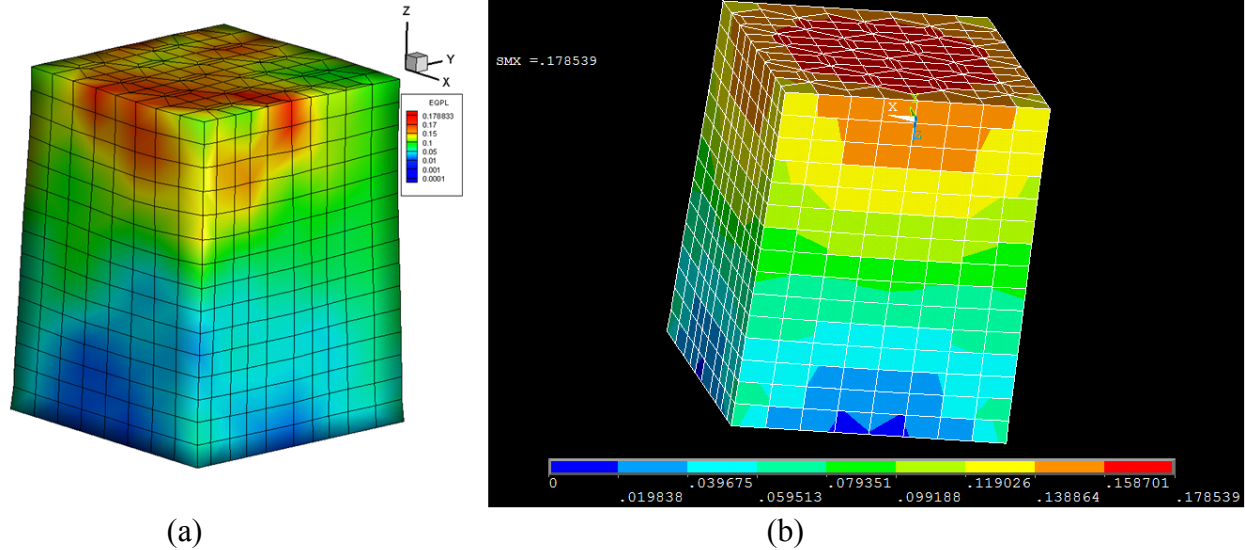
<center>(a)   (b)</center>

Figure9: Plastic strain distribution at 10% total average strain for (a) DDCP-FEM simulations and (b) ANSYS anisotropic multilinear continuum plasticity model. Clearly, the plastic strain evolution in DDCP-FEM simulations is grain-orientation specific in (a) whereas the plastic strain is symmetric about the top and bottom centers of the simulated model in (b). The value of the plastic strain attains its maximum at the top center at ~17.88%. This value coincides with the maximum plastic strain attained in DDCP- FEM simulations (a).

2. Comparison of uniaxial tensile behavior of horizontal and vertical samples modeled using DDCP-FEM

The boundary conditions and the initial dislocation density were the same for both the horizontal and vertical scenarios though the uniaxial strain rate has been applied in a direction perpendicular to the direction as shown in figure 6. The characteristic side-length of the hexagons has been inserted from data in figure 3. The geometry and boundary conditions have been shown in figure10.
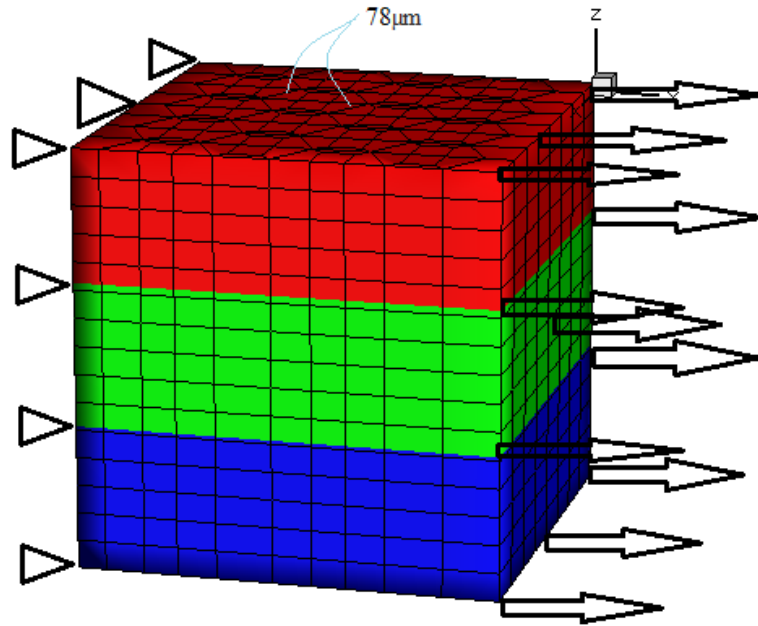
<center>516</center>

Figure10: Uniaxial tensile boundary conditions and included microstructural morphology for horizontal samples. Different colors show grain lengths in the build direction~200µm [9]

The average stress-strain behavior in the loading direction matches well with the experimentally observed true stress-strain curves shown in figure 11 for both the vertical and horizontal scenarios. The yield stress is slightly higher (~50 MPa) in the horizontal case due to delayed onset of slip in the prismatic orientation <a> of the horizontal sample compared to the basal orientation <a> vertical sample as shown in figure 12. The reason why basal orientation of the vertical and prismatic orientation of the horizontal sample have been compared in both the scenarios since they are the dominant slip system orientations in the course of entire deformation as shown in figures 13 and 14 respectively. The change from prismatic dominance in horizontal to basal in the vertical sample is due to the change in the loading direction by 90˚ for similar microstructures in the build direction (z-axis). The maximum plastic deformation also tends to be higher in a horizontal sample (23.14%) when compared to the vertical sample (17.88%) as shown in figure 15 for a total average strain of 10%. The lattice incompatibility or the geometrically necessary dislocations (defined as the spatial gradient of plastic strain measuring the continuum mismatch in the microstructure) tend to concentrate more on prior β grain boundaries leading to Hall–Petch type grain boundary hardening as shown in figure 16. The reason behind the higher capability of the horizontal sample to accommodate plastic strain for same level of average strain compared to the vertical sample is due to a compressive-tensile stress state in the former and a compressive-compressive stress state in the latter leading to a higher deviatoric stress in the former case in the hexagonal plane of the evolved grains during EBM fabrication of the samples. The higher deviatoric stress in the horizontal sample is further explained in figure 17. Due to a higher deviatoric stress in the horizontal sample with lattice incompatibility at grain boundaries, these sites (rectangular planes of hexagonoids) become more prone to delamination at failure strains. This has been already observed in [13].
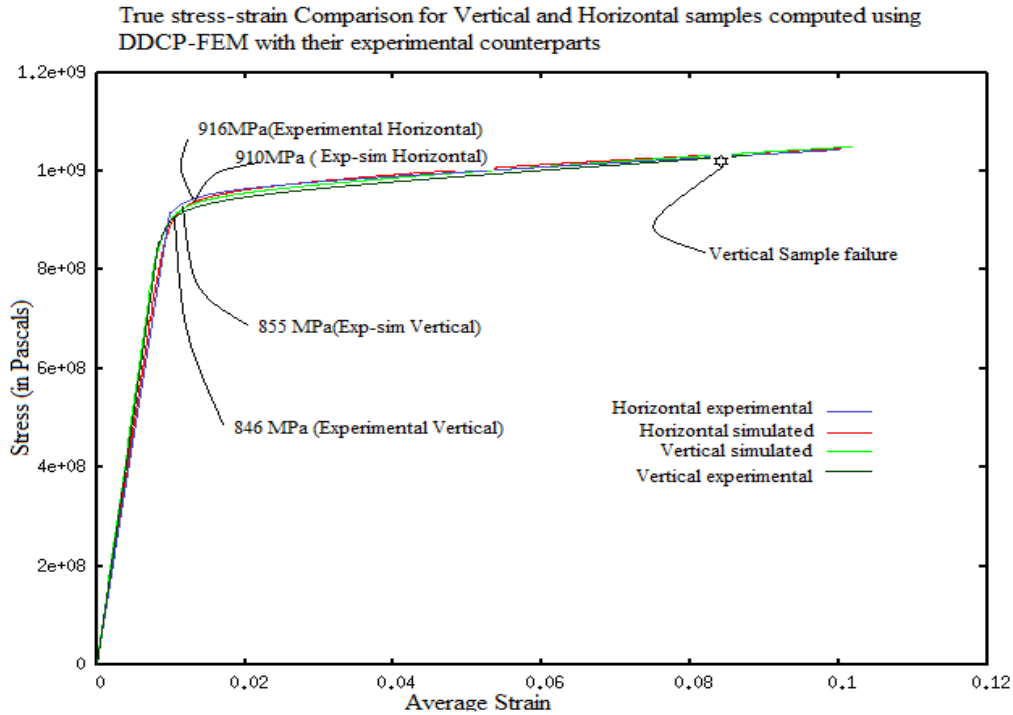
Figure11: True stress-strain match between simulated and experimental for horizontal and vertical samples. Experimentally determined stress-strain curve has been converted into true stress-strain curve.
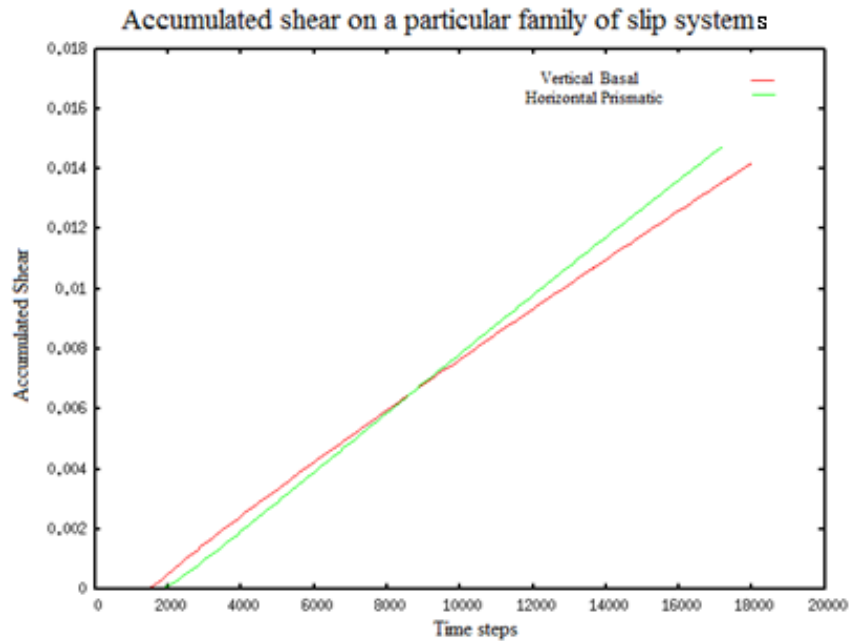

Figure12: Volume-averaged accumulated shear on vertical basal (red) against horizontal prismatic (green) slip systems. The higher yield of the horizontal sample is due to delayed onset of slip on the dominant prismatic slip plane compared to the dominant basal slip plane in the vertical sample.
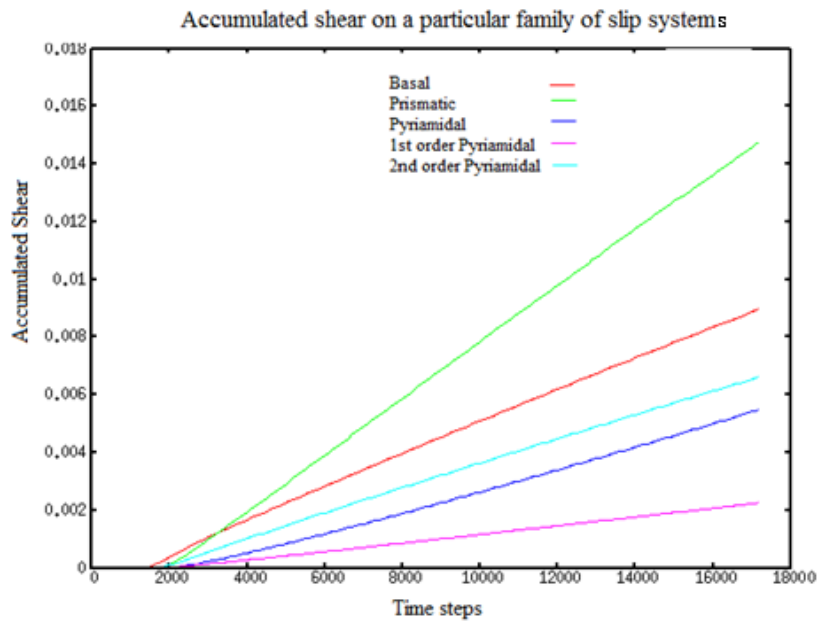
Figure13: Volume-averaged accumulated shear on a particular family of slip systems for a horizontal sample. The dominant slip system is Prismatic <a> (see figure 4).
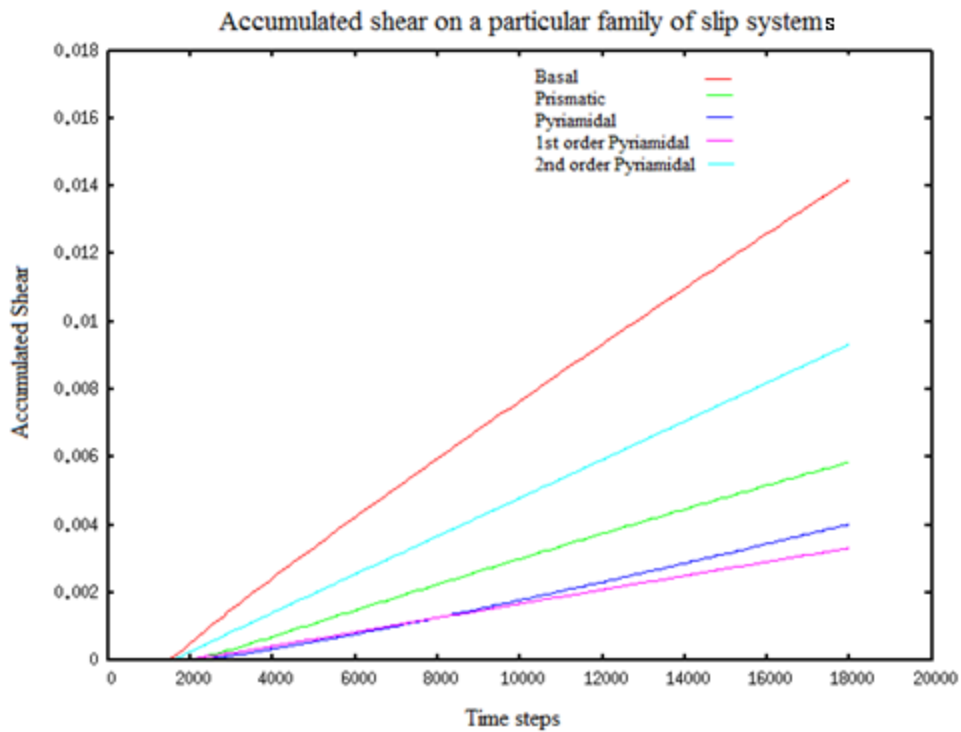

Figure14: Volume-averaged accumulated shear on a particular family of slip systems for a vertical sample. The dominant slip system is Basal <a> (see figure 4).
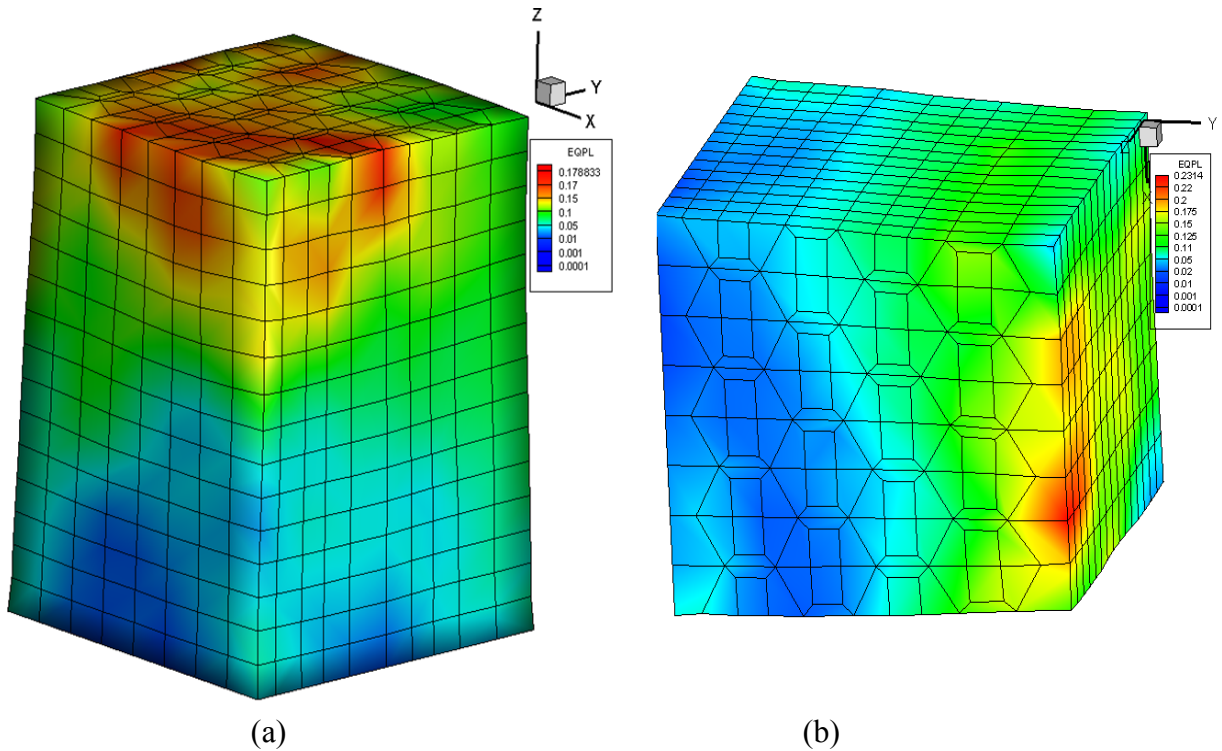
<div align="center">(a)   (b)</div>

Figure15: Plastic strain distribution at 10% average total strain for (a) Vertical sample and (b) Horizontal sample. The local maximum plastic strain in (a) is 17.88%, which is 75% of the maximum plastic strain in (b) (23.14%)

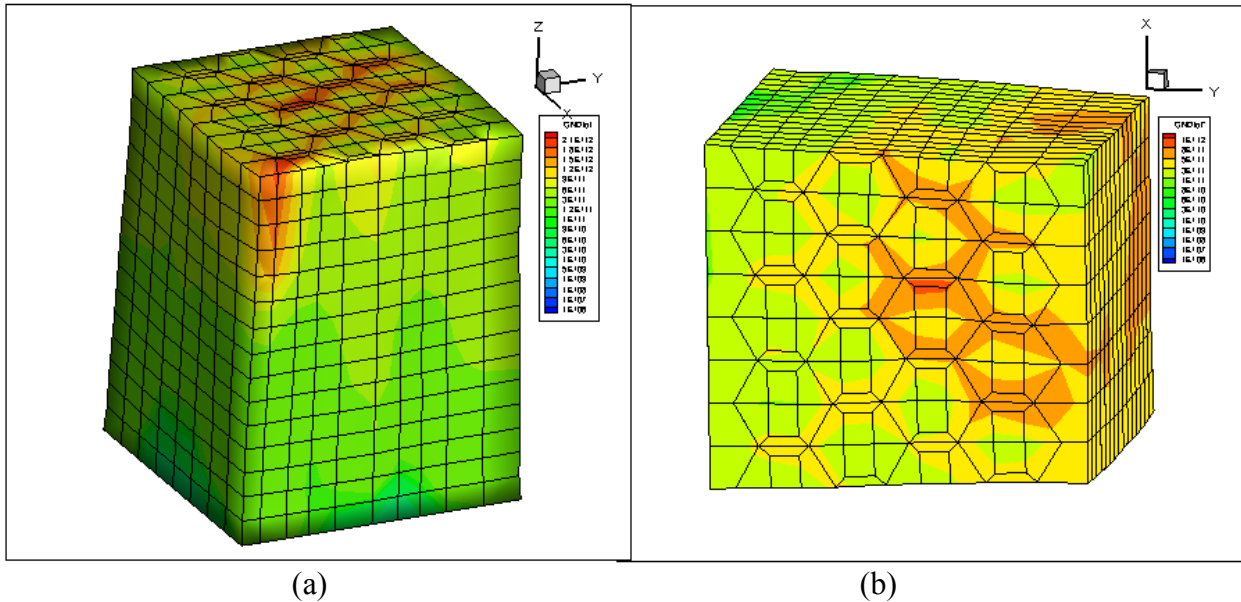<div align="center">(a)   (b)</div>

Figure16: Lattice incompatibility (Geometrically necessary dislocation density) comparison between vertical and horizontal samples. The hardening due to lattice incompatibility tends to be more at the grain boundaries (red regions) compared to the grain interior. A lower maximum magnitude of GND in the horizontal sample $(1\times10^{12}\mathrm{m}^{-2})$ compared to $(2.1\times10^{12}\mathrm{m}^{-2})$ in the vertical sample is due to the stress state shown in figure 17. Also, a lower magnitude of overall GND in the horizontal sample ensures higher ductility and strain to failure since samples tend to

fail beyond a threshold value of GND. Due to a higher concentration of GND in the grain boundaries in the horizontal sample and stress state shown in figure 17, samples tend to delaminate at grain boundaries.

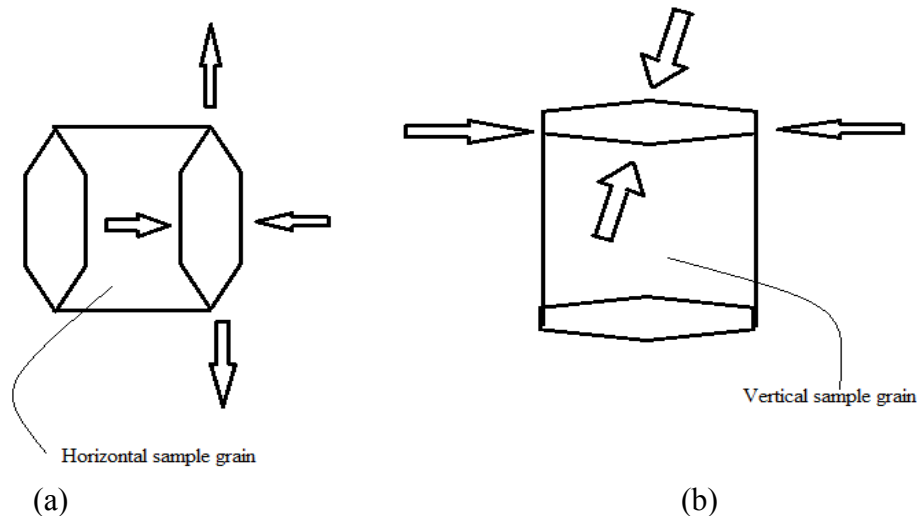(a)   (b)

Figure17: Compressive-tensile and compressive-compressive stress states on the hexagon grain face leading to higher deviatoric stress in horizontal samples, which further leads to higher amounts of plasticity and delamination in the tensile direction along the rectangular grain boundary planes normal to this direction.

3. Comparison of coarse time scale evolutions with fine time scale evolutions for dynamic uniaxial high cycle fatigue

Fatigue simulations have been conducted at a maximum stress of 340 MPa which is also the fatigue limit of the vertically machined samples [13]. The maximum stress of 340 MPa has been employed as a boundary condition in the loading direction shown in figures 6 and 10 for the horizontal and vertical samples respectively. Both the samples have been subjected to a stress ratio of R~0.1 (minimum stress=34 MPa) and their behavior have been simulated for sinusoidal stress cycles between the maximum and minimum stress. The simulation has been conducted in three stages. First, fine time scale DDCP-FEM simulations have been conducted where the samples were initially ramped to the mean stress of 187 MPa in 5 seconds (the dynamic fatigue testing machine ramps the sample to its mean load in 5 seconds [14]) and then sinusoidally oscillated between 340 and 34 MPa at 50 Hz (Time period of oscillations = 20milliseconds). The drawback of these simulations is that the prediction of the deformation behavior is computationally very expensive. In this case, the fine time scale simulations could not be continued beyond 25 cycles since the computational memory was populated and the total simulation time went over the High performance computing thresholds. Therefore, a methodology was required in which the simulations can be conducted in a much faster manner. Henceforth, the APTH operator [11] DDCP-FEM crystal plasticity method has been employed in which first the fine-time scale oscillation problem with zero mean stress and amplitude of 153 MPa (amplitude=340 MPa-187 MPa) was solved for two consecutive cycles and then the evolution of plastic variables per cycle has been inserted into a coarse time scale problem where the entire sample has been ramped to 187 MPa in 5 seconds and then kept constant at that load

throughout the loading history. The coarse time scale problem gives converged results with the initially conducted full fine-time scale results up to 25 cycles, and is 250 times more computationally efficient when compared to the initially conducted fine time scale problem.

It should be noted that the basal slip plane remained the most activated over the entire course of simulations for both the vertical and horizontal samples. The discrepancy in the most activated slip system for the fatigue (basal) with respect to the uniaxial tension (prismatic) problem in the horizontal sample is due to the prior activation of the basal slip plane in tension (red line –basal, green line- prismatic) below and near the yield stress regime in figure 13. Since, the mean stress 187 MPa is much below the yield stress of the sample, therefore the basal slip system is the most activated slip plane in slip for the horizontal sample. Figure 18 shows the volume-averaged cumulative shear on the basal slip plane over the first 25 cycles between the initially conducted fine and coarse time scale simulations for the horizontal samples. The cumulative slip on the most activated slip plane offers the continuum equivalent of cumulative plastic strain as the governing parameter in fatigue for DDCP-FEM based crystal plasticity simulations.
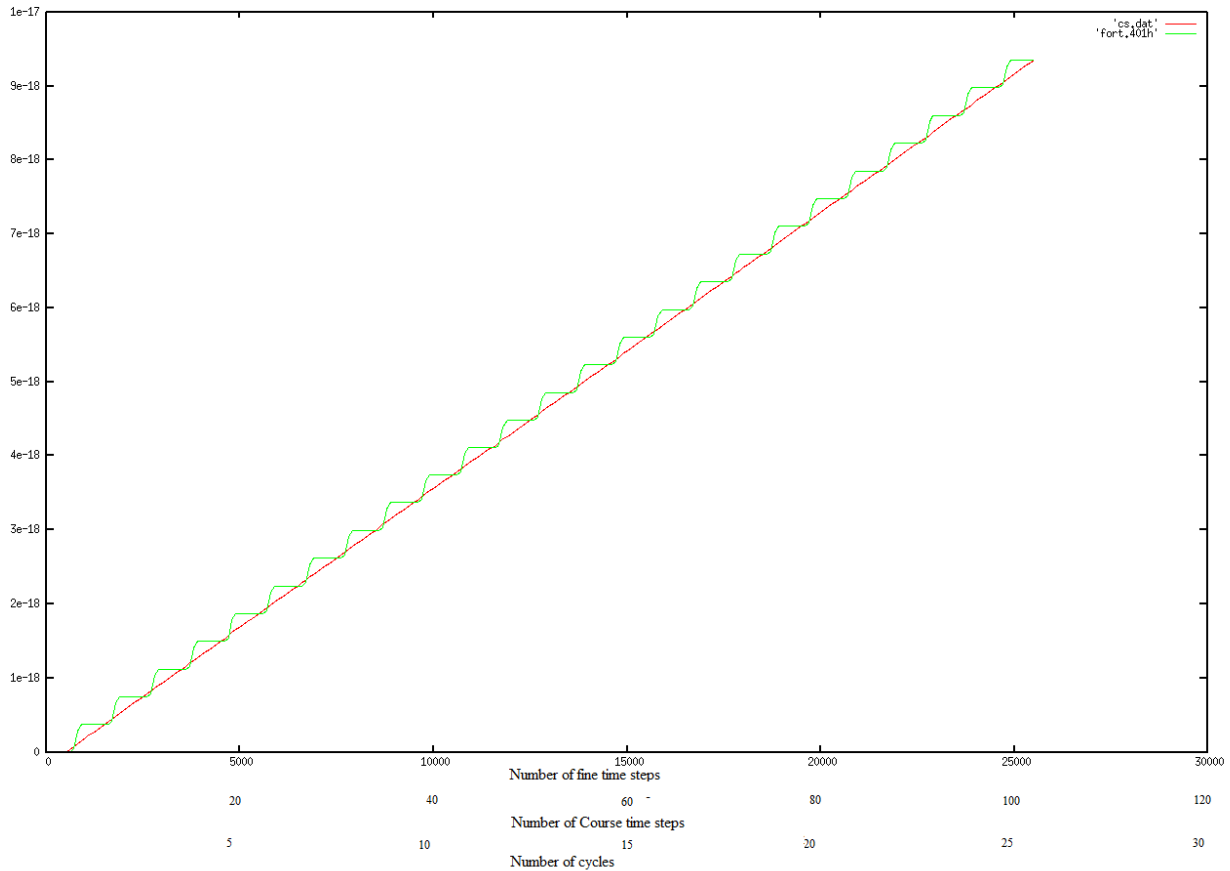

Figure18: Volume averaged cumulative slip (shear) match between the fine (red) and coarse time (green) scale simulations on the basal slip system in the horizontal sample. 100 coarse-time steps are equivalent to 25000 fine time steps for 25 high cycle fatigue cycles. CPU time advantage=250:1.

522

4. Comparison of coarse time scale evolutions with fine time scale evolutions for dynamic uniaxial high cycle fatigue

The coarse time scale volume-averaged cumulative shear in the course of 10 million cycles (maximum number of cycles the dynamic fatigue machine can execute) has been compared between the horizontal and vertical samples. The results are plotted in figure 19. It can be clearly observed that the cumulative plastic strain for the horizontal sample is higher than the vertical sample though the magnitude of the cumulative shear lies in the order of 10^{-12} (very less compared to figure 12) which is significantly less than required for high cycle fatigue crack initiation. It has been shown in [13] that the machined vertical sample has failed at 340 MPa and the horizontal sample has failed at 300 MPa which ensures a brittle crack initiation in both the samples. This has been further confirmed by the microstructure obtained at crack initiation sites in [13] which clearly shows flat shear planes with negligible or no evidence of plasticity. The reasons for brittle crack initiation at a load less than half the yield stress in both the samples are not clear. One of the possible reasons behind premature crack initiation is the improper fabrication of these parts leading to lack of fusion, incomplete melting and balling defects [15].
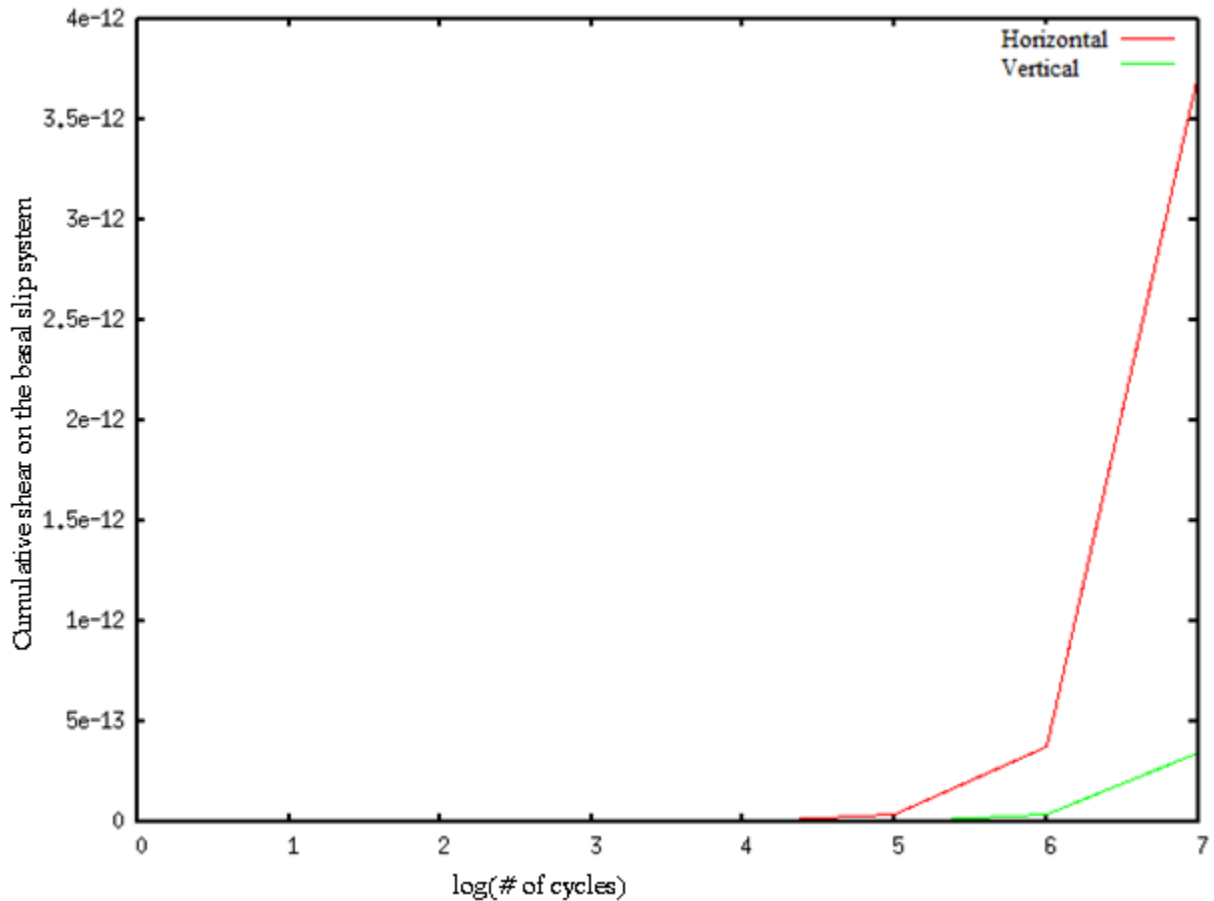

Figure19: Evolution of cumulative shear on basal slip system in horizontal (red) and vertical (green)

Conclusions

The DDCP-FEM simulations successfully predicted the long term deformation behavior of Ti6Al4V parts fabricated using EBM subjected to uniaxial tension (10% strain) and uniaxial fatigue (10 million cycles). The major inferences made during this exercise are as follows:

- Microstructural morphologies as a function of build orientation can be incorporated in DDCP-FEM simulations
- Anisotropic multilinear continuum plasticity fails to explain the plastic strain distribution at the microstructural scale whereas DDCP-FEM simulations can incorporate local microstructural variations in plastic variables such as plastic strain.
- Slip system dominance is a function of build orientation and loading conditions.
- Plastic strain evolution is higher in horizontal samples than vertical samples irrespective of the loading condition.
- Grain delamination in horizontal samples will be at the rectangular facets of the grains due to lattice curvature localization and state of the stress during uniaxial tension.
- The APTH operator coupled with DDCP-FEM can be used to predict the long-term fatigue behavior with 250 times higher computational efficiency than fine-time scale DDCP-FEM simulations.

Future Work

- A process model for solidification during EBM processing will be developed to incorporate non-uniform initial dislocation density in slip systems to initialize the DDCP-FEM simulations.
- Measured grain orientations using electron back scatter diffraction (EBSD) and neutron diffraction (ND) will be converted into Bunge-Euler angle triplets for use as an initial orientation map in the proposed model.
- Future attempts will be made to accommodate the role of the β phase in the microscopic modeling infrastructure.
- Anisotropic multilinear continuum plasticity modeling may fail to explain the microstructural plastic strain distribution, though the 30 times higher computational efficiency can be harnessed with multi-spatial scale simulations.

Acknowledgements

References

1. http://en.wikipedia.org/wiki/Electron_beam_melting
2. Murr, L.E., Quinones, S.A., Gaytan, S.M., Lopez, M.I., Rodela, A., Martinez, E.Y., Hernandez, D.H., Martinez E., Medina, F., and Wicker R.B. Microstructure and mechanical behavior of Ti-6Al-4V produced by rapid-layer manufacturing, for biomedical applications,

Journal of Mechanical Behavior of Biomedical Materials, Volume 2(1), pp.20-32.

3. Pal, D., Behera, S. and Ghosh, S. Crystal Plasticity Modeling of Creep and Microtwinning in Nickel based Superalloys, *United States National Congress on Computational Mecha*nics, Columbus, OH, July 2009.

4. Pal, D. and Stucker, B.E. Dislocation Density Based Finite Element Modeling of Ultrasonic Consolidation, *Solid Freeform Fabrication Symposium Proceedings*, 2010, Austin, TX, August 2010.

5. Pal, D. and Stucker, B.E. Dislocation Density Based Finite Element Modeling of Ultrasonic Consolidation, *Solid Freeform Fabrication Symposium Proceedings*, 2011, Austin, TX, August 2011.

6. Pal, D. Dislocation Density-Based Finite Element Method Modeling of Ultrasonic Consolidation PhD Thesis, Utah State University, August 2011.

7. Pal, D., and Stucker, B.E. Some Studies on Dislocation Density Based Finite Element Modeling of Ultrasonic Consolidation, *Proceedings of the 5th International conference on Virtual and Rapid Prototyping*, Leiria, Portugal, 2011.

8. Pal, D., and Stucker, B.E. Modeling of Ultrasonic Consolidation Using a Dislocation Density Based Finite Element Framework, *Virtual and Physical Prototyping Journal*, Volume 7(1), pp. 65-79, 2012.

9. Safdar, A. Microstructures and surface roughness of EBM produced Ti6Al4V, Licentiate Dissertation, Malmo University, 2010.

10. Staroselsky, A., and Anand, L. A Constitutive Model for HCP Materials Deforming By Slip and Twinning: Application to Magnesium Alloy AZ31B, *International Journal of Plasticity*, Volume 19, 1843-1864, 2003.

11. Pal, D. and Stucker, B.E. Time Homogenization of Al3003 H-18 foils undergoing metallurgical bonding using Ultrasonic Consolidation, *Solid Freeform Fabrication Symposium Proceedings*, 2012, Austin, TX, August 2012 (in communication).

12. ANSYS Theory Manual, Release 11.0, Section 4.2.

13. Khalid Rafi, H., Nadimpalli, K.V., Starr, T.L., and Stucker, B.E. Mechanical Property Evaluation of Ti6Al4V Parts Made Using Electron Beam Melting, *Solid Freeform Fabrication Symposium Proceedings*, 2012, Austin, TX, August 2012 (in communication).

14. 10 KN fatigue testing machine (Model E 10000 Instron)
http://www.instron.us/wa/product/ElectroPuls-E10000-All-Electric-Test-Instrument.aspx

15. Khalid Rafi, H., Nadimpalli, K.V., Starr, T.L., and Stucker, B.E. Defect Formation in EBM Parts Built in Horizontal Orientation, *Solid Freeform Fabrication Symposium Proceedings*, 2012, Austin, TX, August 2012 (in communication).